Advanced Theory and Simulations

ADVANCED THEORY AND SIMULATIONS
www.advtheorysimul.com

RESEARCH ARTICLE OPEN ACCESS

Atomic-Level Insights Into the Initial Oxidative Crystallization of Si(100) to Periodic SiO_x

Divya Srivastava | Antti Lahti | Kalevi Kokko | Marko Punkkinen | Pekka Laukkanen

Department of Physics and Astronomy, University of Turku, Turku, Finland

Correspondence: Divya Srivastava (divya.srivastava@utu.fi)

Received: 16 September 2025 | **Revised:** 17 December 2025 | **Accepted:** 14 January 2026

Keywords: classical molecular dynamics | DFT calculations | electronic band structure | silicon oxidation | simulated LEED

ABSTRACT

MD Simulations based on force fields and first-principles calculations based on density functional theory have been employed to investigate the initial stages of oxidation on silicon (100) surfaces exhibiting a $p(2 \times 2)$ reconstruction when exposed to atomic oxygen. Our results reveal that, when oxygen atoms are sequentially added to energetically preferred sites on the $p(2 \times 2)$ reconstructed Si(100) surface, the lattice maintains its crystallinity for up to three layers, in contrast to the typically observed disordered surface oxide. Detailed atomic and electronic structures of the crystalline SiO_x/Si are presented, which provide a starting point model for the recent measurements of crystalline SiO_x/Si formed under controlled oxidation conditions.

1 | Introduction

The crystalline SiO_x/Si phase holds immense significance and continues to attract substantial attention in both fundamental research and technological applications [1–4]. In contrast, most native SiO_2 and thermally oxidized SiO_2 surfaces are amorphous in nature and inherently contain numerous point defects at the interface. These interfacial defects play a crucial role, as they significantly influence the electronic properties and energy range relevant to device performance. Consequently, understanding and controlling the formation of crystalline SiO_x/Si structures is essential for optimizing their functional behavior in advanced semiconductor technologies.

Mechanisms of silicon oxidation as well as properties of the resulting SiO_2/Si interfaces have attracted enormous interest during several decades due to the significance of SiO_2/Si in semiconductor industry [1, 3, 5–13].

Various atomic structures have been proposed for this interface, including an atomically sharp interface [1] and an extended one with a transition layer [9]. Furthermore, crystalline ordering has also been found for this interface [1, 3] although SiO_2 grown on Si(100) typically has a disordered, amorphous type atomic structure. Indeed, it is widely accepted that the atomic disorder increases significantly immediately when the Si oxidation starts [14–18]. However, an opposite behavior, crystalline order at the oxidized Si surfaces has been recently reported [2, 19]. The quality of the SiO_2/Si interface is significantly influenced by the initial oxidation process [2, 19–22]. During the early stages of oxidation, native oxides, impurities, and defects such as dangling bonds and suboxide states (SiO_x, where $x < 2$), which contribute to interface traps, are easily formed. High-k dielectric films such as HfO_2 or Al_2O_3 have replaced SiO_2 films in many applications. However, the importance of ultrathin (<1 nm) SiO_2 or SiO_x films has increased, as they are often used as interfacial layers in electronics and photonics to reduced harmful surface effects such as leakage current and non-radiative recombination, thereby enhancing overall device performance [23, 24]. A deep understanding of the initial oxidation steps allows one to fine-tune the fabrication process, leading to improved interface properties, lower charge carrier trap densities, and enhanced overall performance of semiconductor devices. The chemisorption of oxygen atoms on the surface of Si(100) is the first step in the formation of

silicon dioxide. Despite considerable progress in understanding the interaction between oxygen and the silicon surface, several questions remain unresolved [25–27].

In this article, we clarify the physicochemical conditions that increase the crystalline degree at the oxidized Si(100) surface and demonstrate an energetically stable atomic structure that could explain recent experimental observations. We employ a novel approach to investigate the initial stage of oxidation of the Si(100) surface with a $p(2 \times 2)$ reconstruction through the sequential addition of oxygen atoms. Neutral atomic oxygen (O) is used as a model species to represent the oxidation process of the Si(100) surface. This simplification provides a reliable and efficient framework for analyzing the resulting atomic configurations and energetics associated with the early formation of SiOx phase on Si(100) surface. For each oxygen atom, we explore the most favorable adsorption positions using density functional theory (DFT) methods using VASP software [28, 29]. The calculation details are described in the methodology section. This theoretical approach captures the thermodynamically favorable pathways for atomic oxygen incorporation into the silicon lattice, without explicitly accounting for kinetic barriers such as O_2 dissociation, oxygen migration, or oxide growth rates. In experimental settings, however, the formation of crystalline SiO_x phases at the Si/SiO_x interface has been observed under high vacuum, relatively low temperatures and controlled oxidation, and is therefore strongly influenced by kinetic limitations.Thus, while the theoretical results indicate which incorporation pathways are energetically preferred, the actual oxidation process is often governed by the rate of O_2 dissociation and atomic mobility. Once dissociation occurs, though, the thermodynamically favorable pathways are expected to strongly influence the earliest stages of oxidation. This study aims to determine: (i) the most stable adsorption site for oxygen, (ii) whether oxygen tends to adsorb on the surface or penetrate into the silicon lattice, (iii) how oxygen adsorption disrupts the silicon lattice, and (iv) the preferred locations for oxygen atoms in cases of partial surface oxidation. These calculations were subsequently extended to larger systems using classical molecular dynamics, and their structural integrity was evaluated at temperatures ranging from 300 to 1700 K to assess their behavior under realistic conditions.

2 | Methodology

For the MD simulations, we evaluated the Tersoff, ReaxFF, and Tersoff_K force fields to determine which provides the best balance between speed and accuracy for modeling the structure and adsorption of atomic oxygen on the Si(100) surface. The surface was created using the optimized bulk geometry of silicon. Bulk silicon, which crystallizes in the diamond cubic structure, was simulated with all three force fields using LAMMPS software [30]. Among these force fields, the Tersoff potential provided lattice parameters that closely matched experimental values. The Si(100) surface was generated by cleaving the optimized bulk structure along the (100) crystallographic plane.The surface model is composed of a slab containing 12 atomic layers, with each layer consisting of 144 silicon atoms. A 10 Å vacuum region is included, and only the top five layers are permitted to relax. It is important to note that, the tested force fields fail to capture the $p(2 \times 1)$ buckled and $p(2 \times 2)$ buckled reconstructions of the Si(100) surface, instead producing a $p(2 \times 1)$ symmetric dimer configuration. The adsorption of atomic oxygen on the Si(100) surface with $p(2 \times 1)$ symmetric dimer configuration was investigated using both the Tersoff and ReaxFF force fields. Both force fields predict the dimer top bridge site, where the oxygen atom adsorbs atop the Si-Si dimer, as the most favorable adsorption site. However, this result does not align with the findings from our DFT calculations. The observed discrepancy between force field-based (e.g., LAMMPS) and DFT-based results for oxygen adsorption on the Si dimer likely arises from limitations in the classical force fields' ability to model electronic effects such as charge transfer and surface reconstruction dynamics. Therefore, to model surface reconstruction and determine the preferred adsorption site for atomic oxygen, DFT calculations were employed. The Si(100) surface was modeled as a 12-layer slab with dimensions 15.4 × 7.7 × 26.4 Å with a 10 Å vacuum region. All surface structures were modeled using a 12-layer slab to allow consistent comparison of relative energies. While slightly thinner than the 14 layers suggested by Sagisaka et al., this thickness is expected to provide reasonably converged structural and energetic differences for studying surface oxidation [31].

The Si(100) surface contains four dimers. The top 5 layers were allowed to relax to capture surface reconstruction and rebonding effects, while the bottom layers were fixed to mimic bulk behavior. Hydrogen atoms terminating the dangling bonds on the bottom surface were allowed to relax to relieve artificial strain from the fixed slab. This passivation permits using a smaller unit cell than a symmetric termination while preventing spurious surface states. It does not affect the relative energies between adsorption geometries on the top surface, as the bottom layers remain identical across all calculations. Moreover, the surface band structure is unaffected by this termination [31]. All DFT calculations were performed using the Vienna ab initio Simulation Package (VASP) with the projector augmented-wave (PAW) scheme and the Perdew–Burke–Ernzerhof (PBE) exchange–correlation functional. A plane-wave energy cutoff of 520 eV was employed. Structural relaxation was performed using a $2X4X1$ Monkhorst–Pack k-point mesh for Brillouin zone (BZ) sampling until the forces on each atom were smaller than 0.0001 eV/Å. The electronic self-consistency criterion was set 10^{-7} eV.

DFT successfully captures the $p(2 \times 1)$ symmetric, $p(2 \times 1)$ buckled, and $p(2 \times 2)$ buckled reconstructions. The primary aim of this study is to explore the adsorption sites for atomic oxygen on the Si(100) surface. It is well established that the Si(100) surface undergoes reconstruction to minimize surface energy. We have examined the $p(2 \times 1)$ symmetric, $p(2 \times 1)$ asymmetric (buckled), and $p(2 \times 2)$ buckled dimer reconstructions, as shown in Figure S1. In the $p(2 \times 2)$ reconstruction, the dimers alternate their buckling orientation within the $p(2 \times 2)$ periodicity (Figure. S1c).

Neutral oxygen atoms were added to the chosen Si(100) surface to model initial oxidation. The overall system remains charge neutral, and the resulting oxygen bonding with the surface is determined self-consistently during relaxation. Thermal stability of the oxidized surface was investigated using LAMMPS [30] with the following parameters. The supercell comprised 12 layers, each containing 96 silicon atoms. The Tersoff potential [27] was employed in all simulation. The oxidized surfaces were simulated

for a total of 40 ps–30 ps for equilibration and 10 ps for production. A target temperature of 2000 K was applied to the top ten layers using an NVT thermostat, while the bottom layers were fixed, effectively maintaining their temperature at 0 K. The average temperature of the full system stabilized at approximately 1700 K, reflecting partial thermal equilibration.

3 | Results and Discussion

In previous studies, the $c(4\times2)$ reconstruction has been identified as the low-temperature phase, typically present in very small quantities, and it gradually transforms into the $p(2\times1)$ phase as the temperature increases to ambient conditions. Although, the $c(4\times2)$ phase, slightly more stable than $p(2\times2)$ by 3 meV per dimer, is not considered due to its minor energetic advantage [32–34]. Among the considered reconstructions- $p(2\times1)$ symmetric, $p(2\times1)$ asymmetric, and $p(2\times2)$ buckled- $p(2\times2)$ Si(100) surface is the most stable, being 0.08 eV per dimer lower in energy than the $p(2\times1)$ phase and 0.27 eV lower than the symmetric structure, in agreement with previous studies [35]. Additionally, the $p(2\times1)$ asymmetric configuration is 0.19 eV per dimer lower in energy than the $p(2\times1)$ symmetric configuration. The surface is semiconducting (see Figure S2b), and the symmetric $p(2\times1)$ reconstruction observed experimentally likely results from temperature averaging; its DOS is presented here for illustrative purposes. All further analysis focuses on the $p(2\times2)$ reconstruction, in line with experimental observations.

3.1 | Atomic Oxygen Chemisorption on Si(100)

Once we select the $p(2\times2)$ surface, we introduce neutral atomic oxygen at various adsorption sites, including on-top, dimer-bridge, dimer-backbond, and exposed back-bond from the second and third subsurface layers on the buckled Si(100) surface with a $p(2\times2)$ periodicity. We examine nine adsorption sites across the top and subsurface layers. Optimization shows that different starting positions often converge to seven unique structures (Figure 1). The most favorable site is the backbond of the down silicon dimer (dDBB), consistent with previous studies [36]. The backbond of the upward silicon dimer (uDBB) incurs an additional energy cost of 0.4 eV. Other metastable sites, approximately 0.2 eV higher in energy than dDBB, include outer backbond sites (BBSL2-SL3) and dimer bridge (DB) positions.

A Bader charge analysis of the pristine Si(100) surface reveals that the down Si atom of the dimer is electron-rich, gaining an additional 0.2 electrons, while the up Si atom is slightly positive, with a deficiency of 0.22 electrons, although uDBB dangling bond is filled. This increased electron density in the down Si atom enhances its favorability for oxygen binding. The down Si atoms bond to the substrate Si atoms at 2.35 Å, while the up Si atoms bond at 2.40 Å. Given that the bulk Si-Si bond length is 2.37 Å, the down Si atoms exhibit stronger bonding to the substrate.

A Bader charge analysis of the dDBB configuration (O adsorbs at the dDBB site of the Si(100) surface) shows that the oxygen gains about 1.60 electrons (from 6.0 to 7.60). The dimer Si atom loses approximately 0.85 electrons, while the second Si atom loses about 0.73 electrons. This asymmetric charge transfer, caused by dimer buckling, results in asymmetric Si–O–Si bond lengths, with the dimer Si–O bond being 0.5 Å shorter than the second Si–O bond. These asymmetric bond lengths improve stress distribution, reducing local stress concentrations and lowering the total energy of the dDBB configuration, thereby enhancing its thermodynamic stability. Therefore, the dDBB site is crucial for silicon oxidation. The oxidation state of the bridging oxygen in Si–O–Si is −2, as the oxygen atom forms two single bonds with the silicon atoms, with bond lengths of 1.65 Å and 1.70 Å.

We now compare the electronic structures, specifically the density of states (DOS), of the pristine surface and the oxygen-adsorbed surfaces for two extreme cases: the most favorable adsorption at the dDBB site and the least favorable adsorption at the uDT site on the Si(100) surface. The calculated total density of states is shown in Figure S3 and discussed in detail. Notably, adsorption of O at the dDBB sites modifies the electronic properties of the system and slightly increases the bandgap compared to pristine (unoxidized) Si(100) surface. In contrast, adsorption at the uDT site reduces the VBM peak height, with only a minimal shift in energy relative to the Fermi level, indicating a weaker perturbation of the local electronic environment and only minor redistribution of valence electrons, resulting in no significant change in the bandgap.

3.2 | Second Oxygen Adsorption on Si(100) With an Occupied dDBB Site

Now, we investigate the adsorption site for a second oxygen atom on Si(100) in the presence of an already occupied backbond of the down silicon dimer (dDBB) site by the first oxygen atom. As shown in Figure 2, the second oxygen atom preferentially inserts into the Si–Si back-bonds of the subsurface layers (BBSL2–SL3). Notably, this adsorption site corresponds to the second most favorable position on a pristine Si(100) surface, suggesting that the presence of the first oxygen atom in the dDBB site enhances the stability of subsurface insertion for subsequent oxidation.

The second lowest energy configuration, with an energy cost of 0.12 eV (S7), occurs when both back-bonds of the downward silicon atoms in the dimers along the row are adsorbed by oxygen atoms. In contrast, if the adsorption occurs at the same dimer in a neighboring site, the energy cost increases to 0.21 eV (S11). It is important to note that all configurations involving the adsorption of oxygen atoms on the up silicon atoms of the dimers are higher-energy configurations. These configurations are not feasible, even at high temperatures, due to their significantly higher energy costs.

However, an exception occurs when the oxygen atom adsorbs directly onto the Si-Si dimer bond, forming a Si–O–Si bridge. While this configuration is more favorable than others involving the up silicon atom, it still comes with an energy cost of 0.27 eV (S1). The silanone structure, in which an oxygen atom forms a double bond with a surface Si atom (O–Si═O), is typically not stable when using atomic oxygen. Even if a silanone configuration is initially constructed, DFT optimization usually leads to rearrangement into a bridging bond (DBB), such as a Si–O–Si bridge, rather than maintaining the Si═O double bond. This behavior

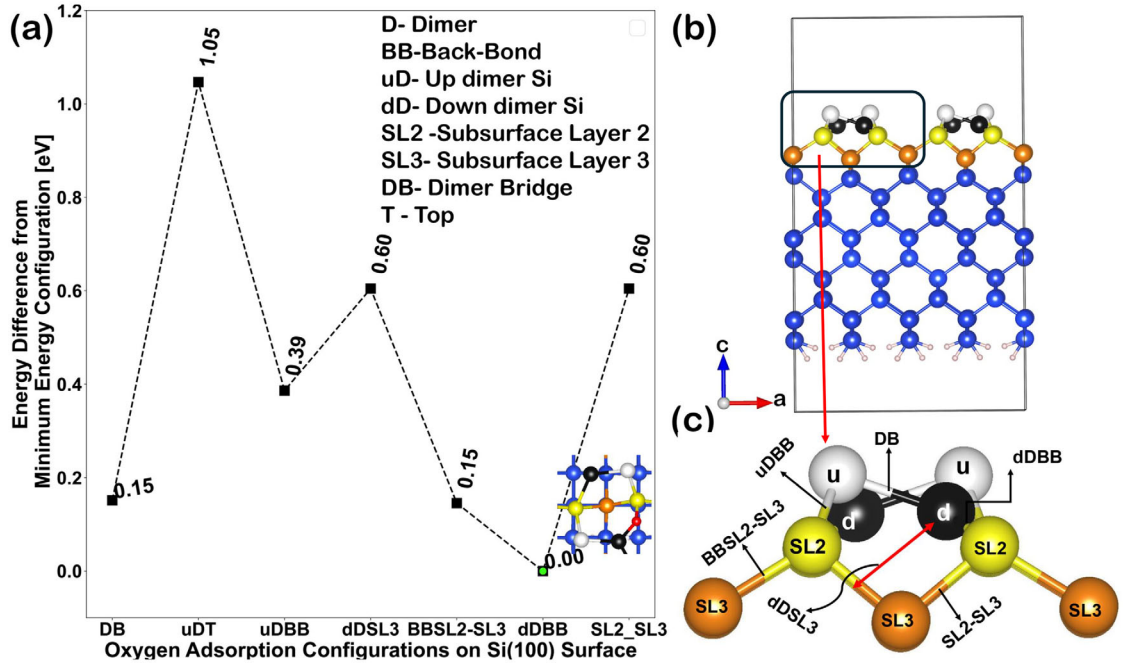

FIGURE 1 | (a) Energy differences corresponding to various oxygen adsorption configurations on the Si(100)$p(2 \times 2)$ surface. The lowest-energy configuration is indicated in neon green. The lines between the energy markers are merely a guide to the eye, highlighting the energy differences. (b) The $p(2 \times 2)$ reconstruction of Si(100) surface, (c) Subsection showing the adsorption sites on the Si(100) surface in side view. White and black spheres represent the up and down Si atoms of the surface dimers, respectively. Yellow (SL2) and orange (SL3) spheres indicate the second and third sub-surface Si layers. The atomic structure in (a) illustrates oxygen adsorbed at the uDBB site.

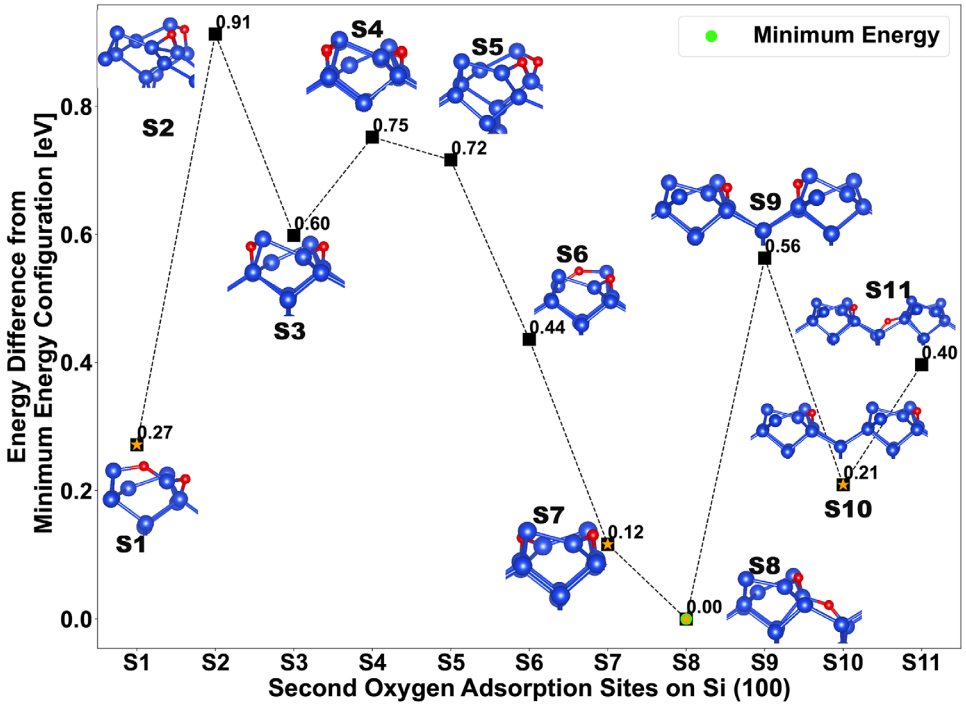

FIGURE 2 | Energy differences for various oxygen adsorption configurations on the Si(100)$p(2 \times 2)$ surface with the dDBB site occupied are presented. The minimum energy configuration is highlighted in neon green and configurations with an energy cost of less than 0.3 eV are highlighted in orange. Small images depict the corresponding atomic structures.

contrasts with oxidation via O_2 dissociation, where Si═O double bond formation on the surface can occur. [37, 38].

To gain insight into the effect of adding a second O atom at the BBSL2–SL3 site (S8) on the electronic structure, we compared the density of states (DOS) of this configuration with that of the surface with a single adsorbed O atom. The calculated DOS is shown in Figure S4. Upon adsorption of the second O atom, the surface bandgap increases further, indicating a cumulative effect of oxygen adsorption on the electronic structure.

3.3 | Identification of the Thermodynamically Preferred Partially Oxidized Si(100) Surface

The oxidation of Si(100) proceeds through distinct chemical and structural stages. Before a continuous SiO_2 layer forms, a partially oxidized silicon surface–typically one or two atomic layers thick–often develops, consisting of a mixture of Si–Si and Si–O bonds. Therefore, to understand the initial stages of oxide growth and the behavior of partially oxidized surfaces that may be observed experimentally, we extend our study to focus on partial oxidation, where one silicon atom in surface dimers is saturated with oxygen, allowing us to analyze the early stages of oxide growth. This configuration is possible at moderate temperatures and low oxygen concentrations, where atoms can diffuse to the most stable sites. The temperature must be high enough to enable diffusion but not too high to change surface energetics. We investigated the partial oxidation of the Si(100) surface using three configurations. In PO1 and PO2, oxygen atoms adsorb on all down dimer back-bonding (dDBB) sites. In PO3, oxygen saturates both dDBB and up dimer back-bonding (uDBB) sites, but only on one side of the dimer. PO2 is the most energetically favorable configuration due to symmetric adsorption, which minimizes surface strain. PO1 also exhibits symmetric adsorption but is slightly higher in energy than PO2. PO3, with asymmetric adsorption and saturation of up silicon atoms, is the least favorable, being 1.5 eV higher in energy than PO2. Notably, we observed this configuration (labeled S7 in Figure 2) as the second lowest-energy structure while investigating the adsorption site for the next oxygen after the dDBB site is saturated. This indicates that the downward-oriented silicon atom within the dimer is the most favorable adsorption site for oxygen atoms on the surface's top layer, adopting a geometry that reduces surface strain. The binding energy of the most stable partially oxidized surface (PO2) is −3.46 eV per oxygen atom, calculated using the equation (S1) given in supporting information. Thus, oxygen adsorption is strongly thermodynamically favorable. Linking the adsorption energy to the equilibrium constant in the Langmuir adsorption model [39], the estimated equilibrium partial pressure of oxygen in PO2 at 1000 K is extremely low, corresponding to the ultra-high vacuum (UHV) regime. This result suggests that oxygen atoms remain adsorbed on the surface, making desorption unlikely at this temperature (Figure 3).

3.4 | Atomic Oxygen Adsorption on PO2 Configuration of Partially Oxidized Si(100)

We aim to investigate where the next O atom prefers to bind on the partially oxidized surface PO2. Does it adsorb at the same site as the second oxygen atom on Si(100), where the first oxygen atom occupies a dimer dDBB site? Or does it prefer to occupy all available sites on the top layer of the surface? To address this, we consider all possible adsorption sites for O, including those on the top layer as well as in the subsurface second layer (SL2) and third layer (SL3). We then optimize the system and compare their energies relative to the most stable configuration (labeled as S5), as shown in Figure S5. The concentration of O atoms on the top layer does not influence the preferred adsorption site for subsequent O atoms when the dDBB sites are occupied. In this case, the next O atom preferentially adsorbs at the BBSL2-SL3 site (labeled S5 in Figure S5). The second most stable configuration, with an energy cost of 0.03 eV (approximately 350 K), corresponds to the formation of a four-membered Si_2O_2 ring (S3). Next, O atoms were added to the most stable configuration (labeled S5 in Figure S5) at various available adsorption sites, including those in the second and third subsurface layers (labeled S1, S2, S3 and S6 in Figure 4) as well as the top layer (S4 and S5 in Figure 4).

The most favorable configuration occurs when a Si atom bonds with three O atoms, forming a SiO_3 unit that shifts upward from the surface plane. Si^{3+} protrusions extending from the silicon surface have been reported in previous studies [12]. Notably, instead of saturating all exposed back-bonds of SL2 and SL3 (as seen in the S1 and S6 configurations), oxygen preferentially bonds with Si atoms that are already coordinated to two oxygen atoms via the dimer back-bond and the exposed SL2-SL3 back-bond. In this arrangement, the oxygen atom integrates into the back-bond of SL2-SL3 inside the lattice. This S2 in Figure 4, now referred to as PO-TSL2, corresponds to the partial oxidation of the top layer and the second subsurface layer. In the PO-TSL2 configuration, the topmost surface retains Si–Si dimers; however, dimers involved in oxidation exhibit a slight elongation compared to pristine dimers. This behavior is consistent with observations by Kuzmin et al. [2], who reported that in crystalline SiOx/Si structures, the topmost Si layer preserves a dimerized (2 × 1) reconstruction even after partial oxidation.

Figure 5 shows a sequence illustrating the evolution of a partially oxidized Si(100) surface to the PO-TSL2 phase, following the PO2 configuration, by sequentially adding oxygen atoms at the most favorable adsorption sites. The binding energy of the S5 configuration is (−3.5 eV) per oxygen atom, while for PO-TSL2, it is (−3.51 eV) per oxygen atom. This suggests that adding oxygen to the silicon lattice is thermodynamically favorable and is not significantly influenced by previously adsorbed oxygen atoms.

3.5 | Electronic Band Structure

It is also interesting to study what kind of effects the oxidation produces on the valence and conduction energy band structure. In the pristine Si(100) surface, the bands near the Fermi level result from silicon dimers (see Figure S6a). Oxygen bonding with silicon shifts surface states within the bandgap, increasing the bandgap, as shown in Figure S6b,c. As oxidation progresses, silicon atoms bonded to oxygen move upward from the original lattice plane. This upward movement causes their localization within the oxide layer, meaning these silicon atoms become confined within the SiO_2 region rather than remaining in the silicon lattice. This phenomenon is more pronounced in the PO-

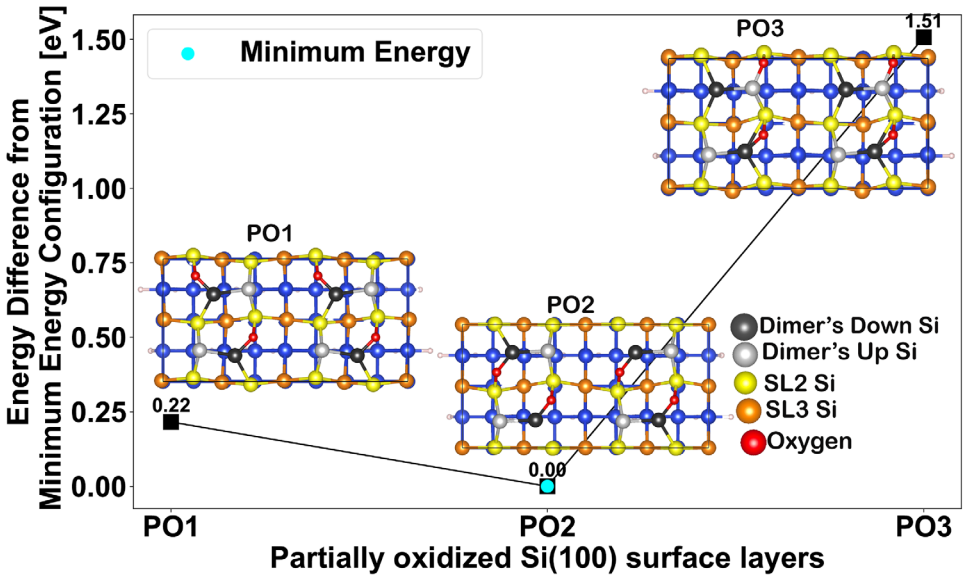

FIGURE 3 | Energy differences for partial oxidation configurations on the Si(100)$p(2 \times 2)$ surface are shown. The minimum energy configuration is highlighted in cyan, with corresponding atomic structures depicted in small images.

TSL2 configuration, as the Si upward shift is greater in PO-TSL2, and this upward shift indicates a reconstruction of the surface structure as the oxide layer forms. Notably, the contribution of oxygen atoms shifts deeper into the valence band with increasing concentration, as oxygen's electro-negativity pulls electron density from silicon, deepening its contribution into the valence band and reducing its impact within 2 eV. The bandgap grows from 0.2 eV in pristine Si(100) to 0.33 eV in Si(100)-PO2 and 0.91 eV in Si(100)-PO-TSL2, indicating a shift from semiconducting to insulating behavior. This trend is consistent with scanning tunneling spectroscopy (STS) measurements conducted before and after oxidation of Si(100), which confirm the development of the electronic bandgap induced by oxidation [2].

3.6 | Validating SiOx/Si Interface Stability on Larger Systems Using LAMMPS

To investigate whether the observed crystalline SiOx/Si structures (PO-TSL2) are artifacts caused by the small periodic cell used in DFT simulations, we complemented our DFT calculations with energy minimization simulations in LAMMPS with the Tersoff potential on a larger supercell consisting of 12 Si layers, each containing 96 Si atoms. All configurations–ordered (labeled Str1 to Str5) and random distributions of oxygen atoms beneath the top layer (labeled "Rand")—were generated starting from the common PO2 structure and then minimized. After structural minimization, configurations that did not retain lattice periodicity were found to be higher in energy–by more than 1 eV–compared to those that maintained periodicity (see Figure 6 and the corresponding structures in Figure S7).

Among the optimized configurations, the SM7:Str5 structure (see Supporting Information), corresponding to the PO-TSL2 configuration obtained from DFT, is the lowest-energy configuration, consistent with our DFT findings.

3.7 | Thermal Stability of the SiOx/Si Interface in Large-Scale Systems Using LAMMPS

To assess the thermal stability of the partially oxidized Si(100) surfaces–Si(100)-PO2 and Si(100)-PO-TSL2–we determined the threshold temperature, defined as the point at which a significant increase in surface disorder begins. We performed molecular dynamics (MD) simulations using LAMMPS with the Tersoff potential. The optimized PO2 and PO-TSL2 structures, along with further details, are provided in the Supporting Information and shown in Figure S8. Temperature-induced structural changes were examined from 300 to 1700 K. No bond breaking or oxygen diffusion was observed within the silicon lattice or at the surface, indicating that the adsorbed oxygen atoms remain stable over this temperature range. While atoms vibrate around their equilibrium positions–particularly with more pronounced and less symmetric motions at the surface due to lower atomic coordination–the overall lattice structure remains intact. This stability is consistent with the Tersoff potential, which predicts a melting point of approximately 2700 K for Si [40]. Although experimental oxidation for crystalline Si/SiO_x phase is typically performed at lower temperatures (approximately 973 K) [2], our simulations suggest that oxygen remains near the top layers without significant diffusion, qualitatively corresponding to the slow oxidation observed experimentally. Thus, the partially oxidized surface is thermodynamically stable, and the structural integrity of the Si lattice is maintained under the simulated conditions.

To quantify surface structural deviations at high temperatures (HT) compared to room temperature (RT), we calculated the disorder parameter (Δ) using the expression: $\Delta = \int_0^\infty [X(RT) - X(HT)]^2 \, dr$, where X represents either the pair-correlation function or X-ray diffraction data. The disorder parameter Δ measures the total structural deviation induced by heating, with results summarized in Table 1. For PO2, significant disorder is observed at 1697 K, while for PO-TSL2, it appears at 1373 K. Although local disorder increases beyond these threshold

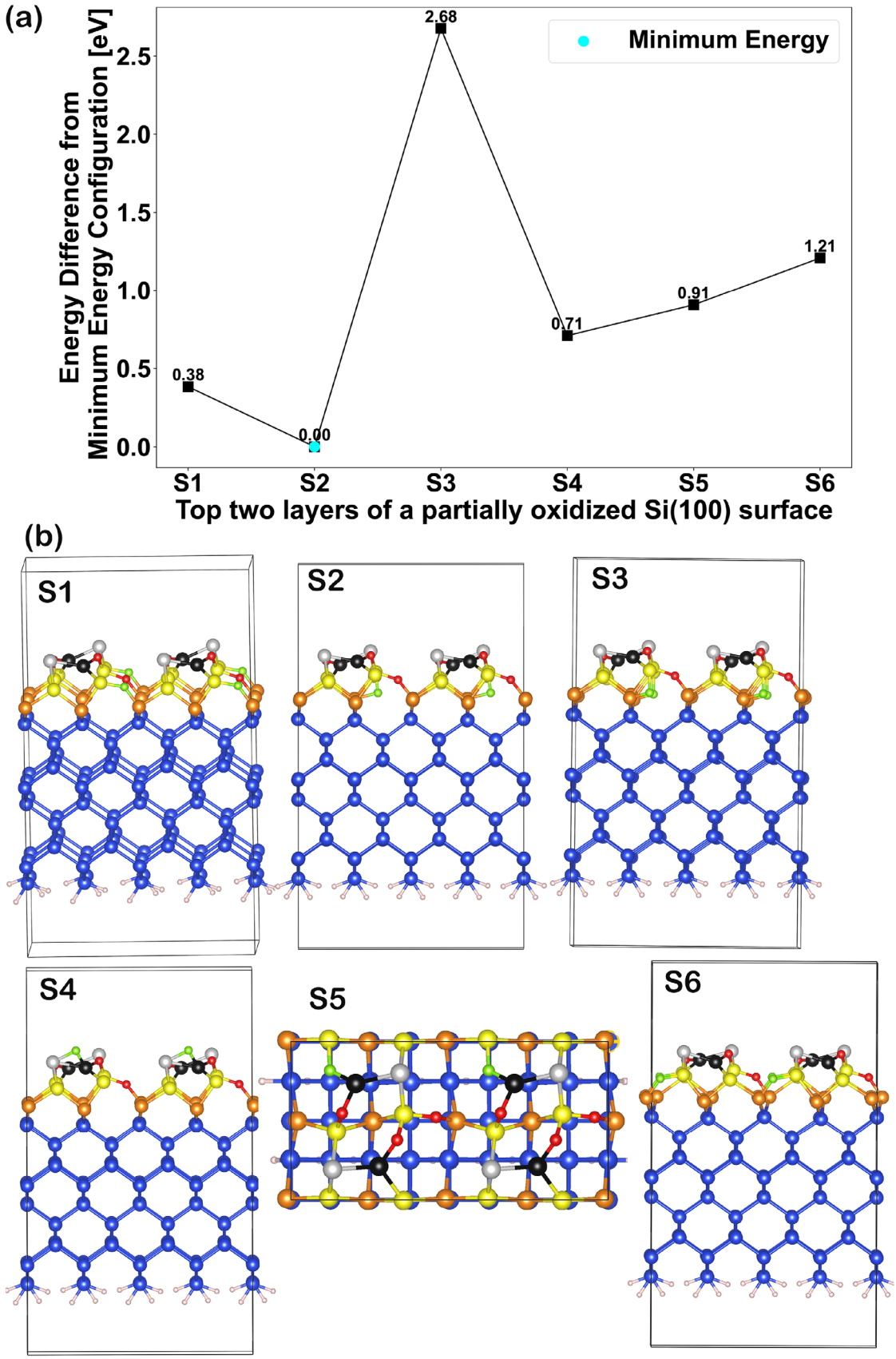

FIGURE 4 | (a) Energy differences for O adsorption at various sites on the S5 configuration are shown in figure SM4, with the minimum energy configuration highlighted in cyan. (b) The atomic structures corresponding to the configurations in (a) are color-coded as follows: white for upward Si of buckled dimers, black for downward Si, yellow for second layer Si, orange for third layer Si, red for oxygen, and neon green for the newly added O atom. The most favorable configuration, S2, is highlighted with a red rectangle.

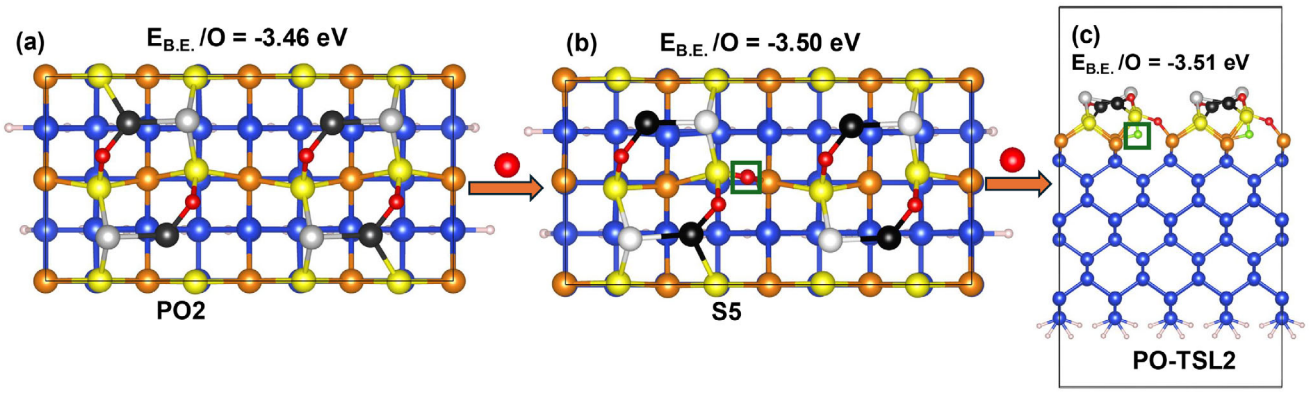

FIGURE 5 | The most favorable adsorption site on the (a) partially oxidized Si(100) surface is shown in (b), with the next most favorable adsorption site for an additional O atom depicted in (c) (PO-TSL2). The newly added oxygen atoms are enclosed in green squares. $E_{B.E.}$ is binding energy and O is oxygen atom.

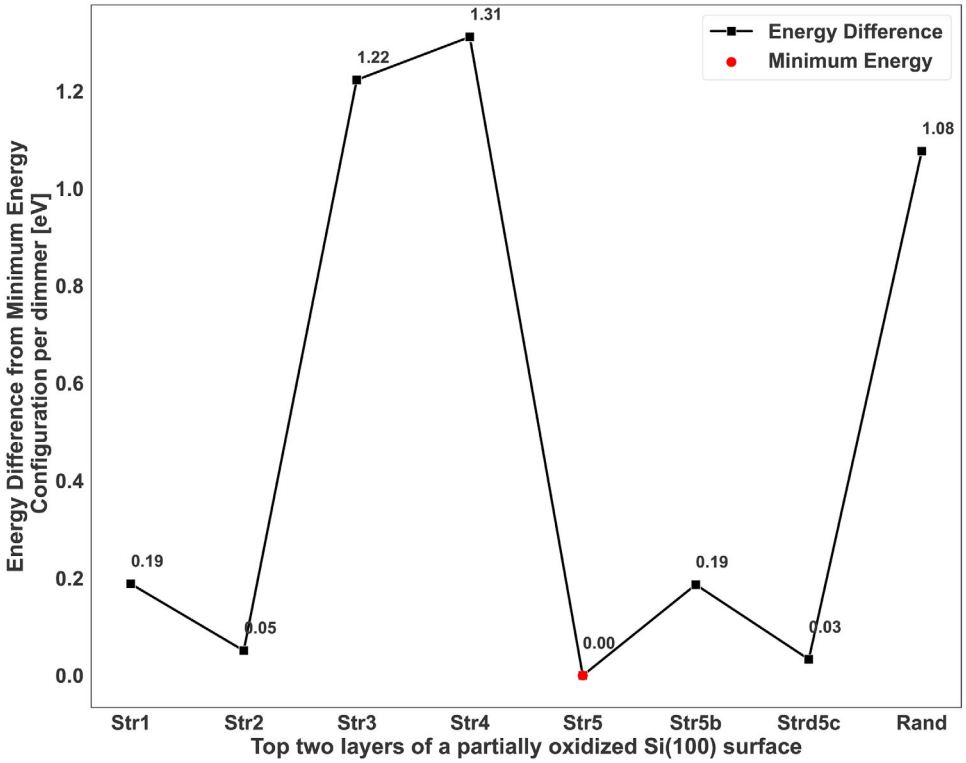

FIGURE 6 | Energy plot showing the relative energy differences of various configurations optimized using LAMMPS with the Tersoff potential. Energies are referenced to Str5, the lowest-energy configuration.

TABLE 1 | Order parameters for Si(100)-PO2/PO-TSL2 surfaces. Values shown as PO2/PO-TSL2.

T (K)	ΔPC(Si-Si)	ΔPC(Si-O)	ΔPC(O-O)	ΔXRD
590	3.85/28.13	29.65/64.80	1.92/561.20	0.000/0.015
812	33.11/44.20	40.52/121.62	1.91/703.96	0.016/0.019
1342/1373	29.62/47.45	50.46/113.38	30.98/772.11	0.015/0.046
1697/1720	126.89/54.61	561.46/218.29	992.06/1080.86	0.076/0.076

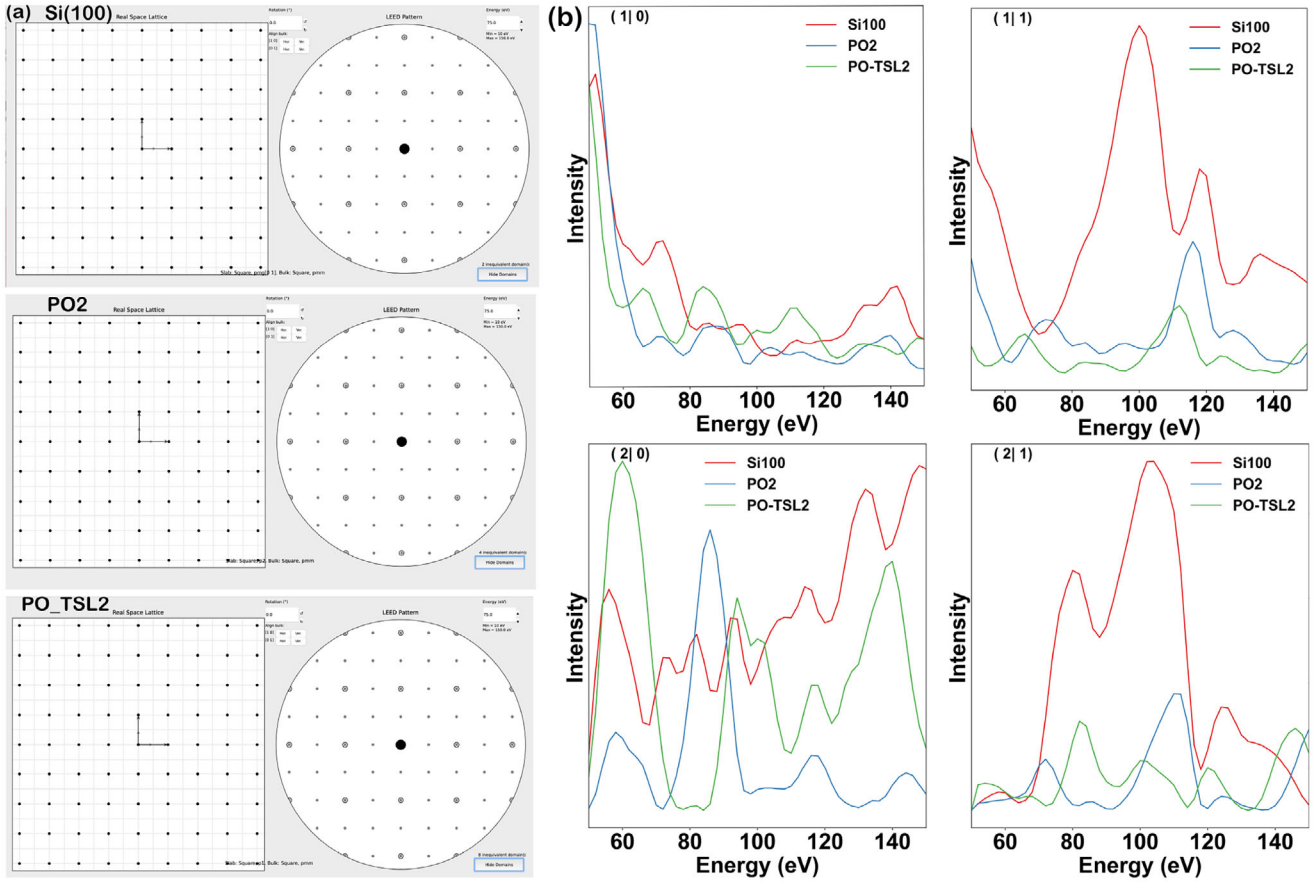

FIGURE 7 | (a) presents the LEED patterns, while Figure (b) shows the corresponding I(V) curves for the pristine, PO2, and PO-TSL2 configurations.

temperatures, the overall crystallinity of the oxidized surfaces remains largely preserved.

3.8 | Simulated Low-Energy Electron Diffraction (LEED)

The simulated low-energy electron diffraction (LEED) patterns and LEED I-V spectra [41, 42] ((details are provided in the Supporting Information)), for the pristine, PO2, and PO-TSL2 configurations are presented in the Figure 7a,b, respectively.

The pristine and oxidized Si(100) surfaces exhibit similar LEED patterns characterized by a $p(2 \times 2)$ reconstruction and bulk-like pmm symmetry, indicating comparable surface periodicities. However, the change in the local chemical environment induced by oxidation progressively reduces the surface symmetry. Oxygen adsorption selectively disrupts symmetry elements such as mirror and glide planes, lowering the surface symmetry from pmg in the pristine Si(100) surface to p2 in the PO2 surface, and eventually to p1 in the PO-TSL2 surface, where only translational symmetry remains. Correspondingly, the LEED spectra reveal an increase in the number of in-equivalent domains–from two in the pristine surface, to four in PO2, and eight in PO-TSL2–reflecting the progressive reduction of surface symmetry and the resulting increase in distinct surface regions related by fewer symmetry operations. Experimentally, LEED shows that the Si(100) surface retains the same $(2 \times 1) + (1 \times 2)$ reconstruction before and after controlled oxidation, indicating no detectable change in the long-range surface periodicity [2].

Figure 7b presents the simulated *I–V* curves calculated at 300 K for pristine and oxidized Si(100) surfaces. The *I–V* spectra of the oxidized surface show substantial deviation from the pristine surface, particularly at higher-order diffraction spots, which are inherently more sensitive to subtle changes in atomic positions. The observed deviation in the *I–V* spectra arises from structural differences in the local surface environment induced by the adsorption of oxygen atoms. The simulated spectra provide valuable reference data for experimentalists, enabling direct comparison with measured *I–V* curves to validate and refine surface structure models.

3.9 | Core-Level Shifts (CLS) via the Initial-State Model

To shed more light on the local symmetries of the oxidized surfaces, we calculate silicon core-level shifts (CLS) using the initial-state model, assuming no final-state effects. Within the framework of DFT, we compute the CLS and evaluate the differences between the oxidized and pristine surfaces (details are provided in the Supporting Information). For the pristine Si(100) surface with buckled dimers, the local chemical environment deviates from that of the bulk crystal. Since the core potential in VASP is negative, a more negative value corresponds to a

deeper potential well and thus a higher core-electron binding energy. The up Si dimer atom exhibits a shallower core potential than in the bulk, while the down Si dimer atom experiences a deeper core potential. Correspondingly, the up Si dimer, with a core-level shift $V^{\mathrm{CLS}} = +0.34\,\mathrm{eV}$, has a lower binding energy than the down dimer Si, which has $V^{\mathrm{CLS}} = -0.51\,\mathrm{eV}$. Because experimental binding energies are positive, a negative core-level shift leads to an increase in the measured binding energy: B.E. $\propto -V^{\mathrm{CLS}}$.

For both PO2 and PO-TSL2 oxidized Si(100) surfaces, oxygen atoms bridge between the down Si dimer atoms and their back-bonded Si neighbors from the second atomic layer. The core-level shifts (ΔV^{CLS}) of these Si atoms are negative relative to the pristine surface, indicating that oxidation leads to a deeper core potential and thus higher binding energy. In the PO2 configuration, all down-Si atoms exhibit a shift of $\Delta V^{\mathrm{CLS}} = -0.47\,\mathrm{eV}$, while the SL2 backbonded Si atoms show a larger shift of −0.56 eV. In contrast, for the PO-TSL2 surface, ΔV^{CLS} decreases to −0.37 eV for those down-Si atoms adjacent to SiO_3 units, whereas the remaining down-Si atoms show shifts comparable to those in PO2. The presence of a highly oxidized neighbor (SiO_3) modifies the local electrostatic environment, reducing the core potential depth and thereby decreasing the magnitude of the core-level shift. The ΔV^{CLS} for SL2 backbonded Si atoms bonded to three oxygen atoms–forming SiO_3 units–reaches −0.89 eV, while those bonded to a single oxygen atom–as in PO2–show a shift of −0.49 eV. These results demonstrate that increased oxidation, particularly the formation of Si–O_3 units, leads to a more negative core potential and thus a deeper binding energy for the affected Si atoms. Therefore, in both PO2 and PO-TSL2 configurations, the oxidation is localized primarily to the down dimer Si atoms and their nearest backbonded neighbors in the second layer, while the up dimer atoms remain largely unaffected. Experimentally, the core-level shifts of the Si 2p level on Si(100) surfaces, relative to Si, are reported as follows: Si^{+} exhibits a shift of –0.95 eV, Si^{2+} –1.75 eV, Si^{3+} –2.48 eV, and Si^{4+} –3.9 eV [12]. The calculated core-level shifts are in qualitative agreement with experimental data, demonstrating that increased oxidation–particularly of Si atoms coordinated to multiple oxygen atoms–leads to more negative binding energies, consistent with substoichiometric oxidation characteristic of early-stage surface oxidation in both PO2 and PO-TSL2 configurations.

4 | Conclusion

In conclusion, our results demonstrate that controlled oxidation plays a crucial role in forming a stable crystalline (SiO_x) layer on the silicon lattice. Oxygen atoms are incorporated sequentially, indicating a stepwise oxidation process, and the ($p(2\times2)$) surface periodicity is preserved even after oxygen penetrates to the third subsurface layer. These atomic-scale insights provide a plausible explanation for the crystalline (SiO_2) observed in experiments involving the oxidation of clean Si under vacuum. Furthermore, band-structure calculations reveal that the bandgap widens as the Si(100) surface transitions from pristine to partially oxidized states. The partially oxidized PO2 and PO-TSL2 surfaces are thermally stable from 300 K up to 1700 K. Local disorder becomes pronounced only near 1700 K for PO2 and around 1400 K for PO-TSL2. Notably, within the PO-TSL2 structure, the (SiO_3) unit remains intact, exhibiting no significant structural changes throughout the entire temperature range of 300–1700 K. The (SiO_3) motif–and the surrounding sites–may serve as preferred anchoring points for incoming oxygen atoms, thereby promoting the formation of thicker (SiO_2) layers. Global optimization can efficiently explore low-energy oxidized Si(100) structures. However, sequential oxidation studies remain essential to capture site-specific adsorption, the formation of intermediate oxide motifs, and metastable surface reconstructions. In the future, it would be desirable to combine these results with machine learning or global optimization methods to study the oxidation of the Si(100) surface using interatomic potentials. This approach would more strongly connect atomistic insights with experimentally relevant oxidation pathways.

Acknowledgements

D.S. acknowledged the Finnish IT Center for Science (CSC) for providing computational resources, as well as the Profi 7 SUSMAT TOT 2608116913 project.

Open access publishing facilitated by Turun yliopisto, as part of the Wiley - FinELib agreement.

Conflicts of Interest

The authors declare no conflicts of interest.

Data Availability Statement

The data that support the findings of this study are available from the corresponding author upon reasonable request.

References

1. A. Ourmazd, D. W. Taylor, J. A. Rentschler, and J. Bevk, "Si -> SiO2 Transformation: Interfacial Structure and Mechanism," *Physical Review Letters* 59 (1987): 213.

2. M. Kuzmin, J.-P. Lehtiö, J. Mäkelä, et al., "Observation of Crystalline Oxidized Silicon Phase," *Advanced Materials Interfaces* 6 (2019): 1802033.

3. A. Munkholm, S. Brennan, F. Comin, and L. Ortega, "Observation of a Distributed Epitaxial Oxide in Thermally Grown sio_2 on si(001)," *Physical Review Letters* 75 (1995): 4254.

4. T. Tanemura, S. Sato, M. Kundu, C. Yamada, and Y. Murata, "Growth of Single-Crystal sio2 Clusters on si(001) Surface," *Journal of Applied Physics* 105, no. 7 (2009): 074310, https://doi.org/10.1063/1.3103331.

5. Y. J. Chabal, *Fundamental Aspects of Silicon Oxidation* (Springer, 2001).

6. G. D. Wilk, Y. Wei, H. Edwards, and R. M. Wallace, "In Situ si Flux Cleaning Technique for Producing Atomically Flat si(100) Surfaces at Low Temperature," *Applied Physics Letters* 70 (1997): 2288.

7. A. Stesmans and V. V. Afanas'ev, "Electron Spin Resonance Features of Interface Defects in Thermal (100)si/sio_2," *Journal of Applied Physics* 83 (1998): 2449.

8. H. Kageshima and K. Shiraishi, "First-Principles Study of Oxide Growth on si(100) Surfaces and at sio_2/si(100) Interfaces," *Physical Review Letters* 81 (1998): 5936.

9. A. Bongiorno, A. Pasquarello, M. S. Hybertsen, and L. C. Feldman, "Transition Structure at the si(100)-sio_2 Interface," *Physical Review Letters* 90 (2003): 186101.

10. T. Yamasaki, K. Kato, and T. Uda, "Oxidation of the si(001) Surface: Lateral Growth and Formation of Pb0 Centers," *Physical Review Letters* 91 (2003): 146102.

11. S. Dreiner, M. Schurmann, and C. Westphal, "Structural Analysis of the sio_2 = si100 Interface by Means of Photoelectron Diffraction," *Physical Review Letters* 93 (2004): 126101.

12. F. J. Himpsel, F. R. McFeely, A. Taleb-Ibrahimi, J. A. Yarmoff, and G. Hollinger, "Microscopic Structure of the sio_2/si Interface," *Physical Review B* 38 (1988): 6084–6096.

13. A. Pasquarello, M. S. Hybertsen, and R. Car, "Interface Structure Between Silicon and Its Oxide by First-Principles Molecular Dynamics," *Nature* 396, no. 6706 (1988): 58–60.

14. T. Engel, "The Interaction of Molecular and Atomic Oxygen With si(100) and Si(111)," *Surface Science Reports* 18 (1993): 93.

15. E. P. Gusev, H. C. Lu, T. Gustafsson, and E. Garfunkel, "Growth Mechanism of Thin Silicon Oxide Films on si(100) Studied by Medium-Energy Ion Scattering," *Physical Review B* 52 (1995): 1759.

16. H. Angermann, T. Dittrich, and H. Flietner, "Investigation of Native-Oxide Growth on HF-Treated si(111) Surfaces by Measuring the Surface-State Distribution," *Appl. Phys. A Sol. Surf.* 59 (1994): 193.

17. F. Fuchs, W. G. Schmidt, and F. Bechstedt, "Initial Stage of si(001) Surface Oxidation From First-Principles Calculations," *Journal of Physical Chemistry B* 109 (2005): 17649.

18. B. N. Jariwala, C. V. Ciobanu, and S. Agarwal, "Initial Oxidation Stages of Hydrogen- and Styrene-Terminated si(100) Surfaces: A Molecular Dynamics Study," *Surface Science* 605 (2011): L61.

19. Z. J. Rad, J.-P. Lehtiö, I. Mack, et al., "Decreasing Interface Defect Densities via Silicon Oxide Passivation at Temperatures Below 450C," *ACS Applied Materials & Interfaces* 12 (2020): 46933.

20. A. Yoshigoe, K. Moritani, and Y. Teraoka, "Real-Time Observation of Initial Thermal Oxidation Using O2 Gas on si-2p Photoemission Spectroscopy," Vol. 216 (2003): 388–394.

21. S. M. Hu, "Anomalous Temperature Effect of Oxidation Stacking Faults in Silicon," *Applied Physics Letters* 27 (1975): 165–167.

22. N. F. Mott, S. Rigo, F. Rochet, and A. M. Stoneham, "Oxidation of Silicon," *Philosophical Magazine B: Physics of Condensed Matter; Statistical Mechanics, Electronic, Optical and Magnetic Properties* 60 (1989): 189–212.

23. F. Feldmann, M. Bivour, C. Reichel, M. Hermle, and S. W. Glunz, "Passivated Rear Contacts for High-Efficiency n-Type si Solar Cells Providing High Interface Passivation Quality and Excellent Transport Characteristics," *Solar Energy Materials and Solar Cells* 120 (2014): 270–274.

24. S. S. Cheema, N. Shanker, L.-C. Wang, et al., "Ultrathin Ferroic HfO2-ZrO2 Superlattice Gate Stack for Advanced Transistors," *Nature* 604 (2022): 65–71.

25. V. Barone and F. Lelj, "Chemisorption of Atomic and Molecular Oxygen on the (100) Surface of Silicon: A Theoretical Study," *Surface Science* 162 (1985): 230–238.

26. K. Kato, T. Uda, and K. Terakura, "Backbond Oxidation of the si(001) Surface: Narrow Channel of Barrierless Oxidation," *Physical Review Letters* 80, no. 9 (1998): 2000–2003.

27. Y. Tu and J. Tersoff, "Structure and Energetics of the si-sio_2 Interface," *Physical Review Letters* 84 (2000): 4393–4396.

28. G. Kresse and J. Furthmüller, "Efficient Iterative Schemes for Ab Initio Total-Energy Calculations Using a Plane-Wave Basis Set," *Physical Review B* 54, no. 16 (1996): 11 169–11 186.

29. G. Kresse and D. Joubert, "From Ultrasoft Pseudopotentials to the Projector Augmented-Wave Method," *Physical Review B* 59, no. 3 (1999): 1758–1775.

30. S. Plimpton, "Fast Parallel Algorithms for Short-Range Molecular Dynamics," *Journal of Computational Physics* 117 (1995): 1–19, LAMMPS Molecular Dynamics Simulator, http://lammps.sandia.gov/.

31. K. Sagisaka, J. Nara, and D. Bowler, "Importance of Bulk States for the Electronic Structure of Semiconductor Surfaces: Implications for Finite Slabs," *Journal of Physics: Condensed Matter* 29 (2017): 145502.

32. A. Ramstad, G. Brocks, and P. J. Kelly, "Theoretical Study of the si(100) Surface Reconstruction," *Physical Review B* 51 (1995): 14 504–14 520.

33. K. C. Low and C. K. Ong, "Electronic Structure of the Si(100) C(4 × 2) and P(2 × 2) Surfaces," *Physical Review B* 50 (1994): 5352–5357.

34. Y. J. Lee, S. Kim, C.-S. Hwang, C. Lee, and C. Hwang, "Reconstruction on si(100) Surfaces," *Physical Review B* 50 (1994): 11 204–11 207.

35. A. Ramstad, G. Brocks, and P. J. Kelly, "Theoretical Study of the si(100) Surface Reconstruction," *Physical Review B* 51 (1995): 14 504–14 523.

36. T. Uchiyama and M. Tsukada, "Atomic and Electronic Structures of Oxygen-Adsorbed si(001) Surfaces," *Physical Review B* 53 (1996): 7917–7922.

37. Y. J. Chabal, K. Raghavachari, X. Zhang, and E. Garfunkel, "Silanone (Si = O) on si(100): Intermediate for Initial Silicon Oxidation," *Physical Review B* 66 (2002): 161315.

38. A. Hemeryck, A. J. Mayne, N. Richard, et al., "Difficulty for Oxygen to Incorporate Into the Silicon Network During Initial O2 Oxidation of si(100)-(2 × 1)," *The Journal of Chemical Physics* 126, no. 11 (2007): 114707.

39. H. Swenson and N. P. Stadie, "Langmuir's Theory of Adsorption: A Centennial Review," *Langmuir* 35 (2019): 5409–5426.

40. S. J. Cook and P. Clancy, "Comparison of Semi-Empirical Potential Functions for Silicon and Germanium," *Physical Review B* 47 (1993): 7686–7699.

41. K. Heinz and K. Müller, "LEED Intensities – Experimental Progress and New Possibilities of Surface Structure Determination," in *Structural Studies of Surfaces*, ser. Springer Tracts in Modern Physics, vol. 91 (Berlin, Heidelberg: Springer, 1982), 1–33.

42. P. Laukkanen, J. Sadowski, and M. Guina, "Surface Studies by Low-Energy Electron Diffraction and Reflection High-Energy-Electron Diffraction," in *Semiconductor Research: Experimental Techniques*, ser. Springer Series in Materials Science, A. Patanè and N. Balkan, Eds. (Springer-Verlag, 2012), 1–21.

Supporting Information

Additional supporting information can be found online in the Supporting Information section.

Supporting File: adts70309-sup-0001-SuppMat.pdf.